ELSEVIER

NeuroImage

www.elsevier.com/locate/ynimg
NeuroImage 30 (2006) 544 – 553

Neuronal chronometry of target detection: Fusion of hemodynamic and event-related potential data ☆

V.D. Calhoun,[a,b,c,*] T. Adali,[d] G.D. Pearlson,[a,b,c] and K.A. Kiehl[a,b]

[a]*Olin Neuropsychiatry Research Center, Institute of Living, Hartford, CT 06106, USA*
[b]*Dept. of Psychiatry, Yale University School of Medicine, New Haven, CT 06520, USA*
[c]*Dept. of Psychiatry, Johns Hopkins University, Baltimore, MD 21205, USA*
[d]*Dept. of CSEE, University of Maryland Baltimore County, Baltimore, MD 21205, USA*

Received 5 May 2005; revised 22 June 2005; accepted 23 August 2005
Available online 24 October 2005

Event-related potential (ERP) studies of the brain's response to infrequent, target (oddball) stimuli elicit a sequence of physiological events, the most prominent and well studied being a complex, the P300 (or P3) peaking approximately 300 ms post-stimulus for simple stimuli and slightly later for more complex stimuli. Localization of the neural generators of the human oddball response remains challenging due to the lack of a single imaging technique with good spatial and temporal resolution. Here, we use independent component analyses to fuse ERP and fMRI modalities in order to examine the dynamics of the auditory oddball response with high spatiotemporal resolution across the entire brain. Initial activations in auditory and motor planning regions are followed by auditory association cortex and motor execution regions. The P3 response is associated with brainstem, temporal lobe, and medial frontal activity and finally a late temporal lobe "evaluative" response. We show that fusing imaging modalities with different advantages can provide new information about the brain.

Keywords: fMRI; Auditory oddball; Independent component analysis; P3

Introduction

The processing of auditory stimuli presented during an 'oddball' task requires detection of infrequent target stimuli within the context of frequently presented standard stimuli (Sutton et al., 1967; Polich and Kok, 1995)—for example, the detection of an occasional high-pitched tone in a sequence of low-pitched tones. Brain activity during oddball tasks is frequently measured by averaging task-related electroencephalogram (EEG) recordings to produce event-related potentials (ERPs). These brain responses are labeled either by their polarity and approximate time to peak (e.g., P300) or by their ordinal position following the stimulus onset (e.g., P3 for the third positive peak or N2 for the second negative peak). Over three decades ago, it was reported that low probability, task relevant auditory stimuli elicited a characteristic ERP waveform that includes several meaningful components, including the mismatch negativity (Naatanen and Alho, 1995) related to sensory trace memory, the N2 related to matching stimuli to an internally-generated contextual template (Gehring et al., 1992), and the P3, which is generally thought to reflect directed, effortful processing (Knight and Nakada, 1998) and contextual updating of working memory processes (Donchin and Coles, 1988). It is now known that the amplitude and latency of the P3 are modulated by a variety of experimental manipulations, including stimulus probability, task difficulty, and task demands (Donchin and Coles, 1988). Moreover, it is believed that there are multiple subcomponents of the P3 (i.e., P3a, P3b, P3f) (Dien et al., 2004). These findings support the interpretation that the P3 reflects processes related to attention, decision making, and memory updating. The P3 also has been shown to be abnormal in many clinical conditions, including schizophrenia, depression, Alzheimer's disease, and psychopathy (McCarley et al., 1991; Ford et al., 1994; Kiehl et al., 1999).

Work using principal component analysis (PCA) (Brown et al., 1979; Kayser et al., 1998; Kayser and Tenke, 2003) or independent component analysis (ICA) (Debener et al., 2005) has decomposed ERP waveforms into specific components corresponding to the various parts of the ERP waveform. There are a number of scalp-recorded components for which generators have been confidently identified, including the lateralized readiness potential (LRP), the error-related negativity (ERN), the P50, the P100, the N100, and the mismatch negativity (MMN) as well as a number of earlier sensory components. The main generators of the P3 have been identified by Halgren et al. (1998) using a combination of techniques including EEG, magnetoencephalography (MEG), and

☆ Previously submitted to Neuroimage on 6 May 2005. This version submitted 18 June 2005, Accepted 23 Aug 2005.

* Corresponding author. Olin Neuropsychiatry Research Center, Institute of Living, 200 Retreat Ave., Hartford, CT 06106, USA.
E-mail address: vince.calhoun@yale.edu (V.D. Calhoun).

Available online on ScienceDirect (www.sciencedirect.com).

1053-8119/$ - see front matter © 2005 Elsevier Inc. All rights reserved.
doi:10.1016/j.neuroimage.2005.08.060

structural MRI. MEG, like EEG, is a direct measure of neuronal activity with excellent temporal resolution, but variable spatial resolution (from mm to cm range).

EEG/MEG and functional magnetic resonance imaging (fMRI) are thought to have complementary strengths and weaknesses. The strength of techniques such as EEG and MEG is clearly in their temporal resolution and the ability to measure neuronal activity directly. In contrast, fMRI has excellent uniform spatial resolution but measures an indirect metabolic correlate of neuronal function—the blood oxygenation level dependence (BOLD). To date, over a dozen fMRI experiments have employed oddball paradigms to examine target-related neural activity (McCarthy et al., 1997; Kiehl and Liddle, 2001; Clark et al., 2001). A recent large scale (n = 100) auditory oddball fMRI study found highly reliable activation in 38 regions for target detection (Kiehl et al., 2005). Regions activated during processing of target stimuli included portions of bilateral temporal lobes, lateral frontal, lateral parietal, and thalamus, amygdala, and cerebellum, as well as motor-related areas (Kiehl et al., 2005). The temporal resolution of fMRI, though challenged by the slow hemodynamic response, has been used to examine delay differences on the order of 100–200 ms (Calhoun et al., 2000; Saad et al., 2001) which is helpful, but much less precise than the temporal information provided by EEG. In summary, though fMRI and ERP both provide spatial and temporal information, the strengths of each technique differ. Thus, an approach which combines fMRI and ERP can potentially draw upon the strengths of each and provide additional information not afforded by either technique alone. Despite this obvious motivation; combining these two modalities has proven technically challenging.

Previously, several different approaches have been used to combine electromagnetic and hemodynamic data. Initial work focused upon constraining the electromagnetic source locations using fMRI or structural MRI data (Menon et al., 1997; Opitz et al., 1999; Dale et al., 2000), to improve spatial estimates. More recently, correlations between hemodynamic and electrical activity have been observed in animals by combining single cell recording with fMRI techniques (Logothetis et al., 2001). In humans, correlations between fMRI and ERP peak amplitude (Arthurs et al., 2000; Horovitz et al., 2002; Mathalon et al., 2003; Arthurs and Boniface, 2003) or ERP power (in certain frequency bandwidths) (Goldman et al., 2002) or direct multidimensional estimation (Martinez-Montes et al., 2004) have enabled inferences to be made about both hemodynamic and electrical sources of target detection. However, the connection between different components of the ERP waveforms (as opposed to summary measures like peak amplitude) and fMRI spatial maps has not yet been examined.

Independent component analysis, a method which maximizes the independence between components, has been successfully used on both fMRI and EEG data separately. The ICA approach models spatiotemporal data as a linear combination of spatial maps and time courses while attempting to maximize the independence between either the maps (spatial ICA) or the time courses (temporal ICA). ICA was originally developed to solve problems similar to the "cocktail party" problem in which many people are speaking at once and multiple microphones each record mixtures of the speaker's voices (Bell and Sejnowski, 1995). The ICA algorithm, assuming independence in time (independence of the voices), can separate mixed signals into individual sources (voices). ICA was next applied to the analysis of EEG data in which a set of signals, one from each electrode, are separated into temporally independent groups (Makeig et al., 1997). The first application of ICA to fMRI data used spatial-ICA (McKeown et al., 1998) to determine spatially distinct brain networks. It is possible to perform ICA in either the temporal or spatial domain (Calhoun et al., 2001). For ERP data, it is more common to use *temporal* ICA whereas for fMRI data it is more common to use *spatial* ICA for various reasons, but primarily because of the larger number of data points in these domains (Calhoun et al., 2001). However, what has not been attempted is a joint estimation of the temporal components of the ERP response (Kayser and Tenke, 2003; Debener et al., 2005) and the spatial components revealed by fMRI (Kiehl et al., 2001). Such an approach has the potential to reveal electrical sources which may not be readily visible to scalp ERPs or to expose brain regions that have participatory roles in source activity, but may not themselves be generators of the detected electrical signal (Martinez-Montes et al., 2004).

In this work, we jointly performed spatial ICA of fMRI data and temporal ICA of ERP data in a group of 23 healthy participants in order to derive a spatiotemporal decomposition consisting of fMRI components indicating *where* the signal is changing and ERP components indicating *when* the signal is changing. In Fig. 1, we present an illustration of our approach. The initial step involves computing, for a given stimulus, the time locked ERP waveform and fMRI activation map, for each participant (i.e., the input data). Our approach exploits inter-subject covariation between temporal parts of the ERP waveform and spatial locations of the fMRI maps (an example is depicted in Fig. 1a as low intensity regions for a given brain which are specific to a particular pattern of "where" and "when"). The ICA algorithm jointly computes linked temporally independent ERP components and spatial independent fMRI components (Fig. 1b). The results can also be visualized by computing spatiotemporal "snapshots" (Fig. 1c) providing a way to examine the dynamic interplay between hemodynamic and electromagnetic sources. Results are displayed as time varying spatial maps (linear combinations of the fMRI component images) along with the ERP components (Fig. 5). It is also straightforward to plot, for a given spatial location, ERP time courses (computed from a linear combination of the estimated ERP components; Fig. 6).

Our approach thus enables inferences to be made using estimated associations between fMRI hemodynamic sources and ERP electromagnetic sources.

Methods

Participants

Participants were recruited via advertisements, presentations at local universities, and by word-of-mouth. Twenty-three healthy participants (15 male, 8 female, Age 41 ± 14 years) provided written, informed, IRB-approved consent at Hartford Hospital and were compensated for their participation. Prior to inclusion in the study, healthy participants were screened to ensure they were free from DSM-IV Axis I or Axis II psychopathology [assessed using the SCID (Spitzer et al., 1996) and also interviewed to determine that there was no history of psychosis in any first-degree relatives]. All participants had normal hearing (assessed by self-report), no history of any central nervous system disease, and were able to perform the task successfully during practice prior to the scanning session.

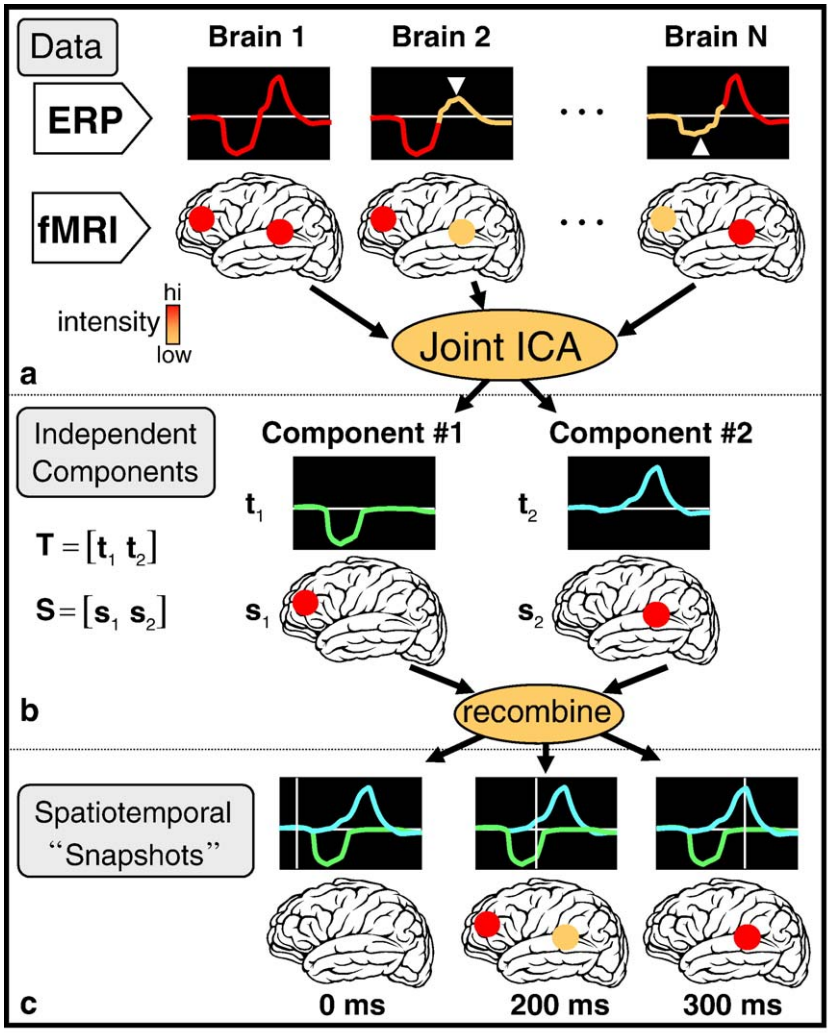

Fig. 1. Illustration of joint ICA fMRI/ERP data fusion: motivating example in which (a) portions of the brain in the fMRI data are shown to be associated with portions of the time courses in the ERP data. Using joint estimation of spatial and temporal independence captures this variation and results in a set of joint components (b) which indicate, for each component, *where (fMRI)* and *when (EEG)* the activity was occurring. The matrices **T** and **S** represent all the temporal and spatial components, with $\boldsymbol{t}_i$ and $\boldsymbol{s}_i$ being a fused spatial and temporal pair for the ith component. Once the components are estimated, one can recombine them in order to examine the dynamic interplay between space and time (c).

Experimental design

The auditory oddball task (AOD) requires subjects to press a button when they detect an infrequent sound within a series of regular and different sounds. Three stimuli are presented; frequent low-tone stimuli (standards), infrequent task-irrelevant stimuli (novels), and infrequent task-relevant stimuli (targets) requiring a button-press response. In the present experiment, the standard stimulus was a 500 Hz tone, the target stimulus was a 1000 Hz tone, and the novel stimuli consisted of nonrepeating random digital noises (e.g., tone sweeps, whistles) (Fig. 2). Two runs of auditory stimuli were presented to each participant by a computer stimulus presentation system via insert earphones embedded within 30 dB sound attenuating MR compatible headphones.

The target and novel stimuli each occurred with a probability of 0.10; the nontarget stimuli occurred with a probability of 0.80. The

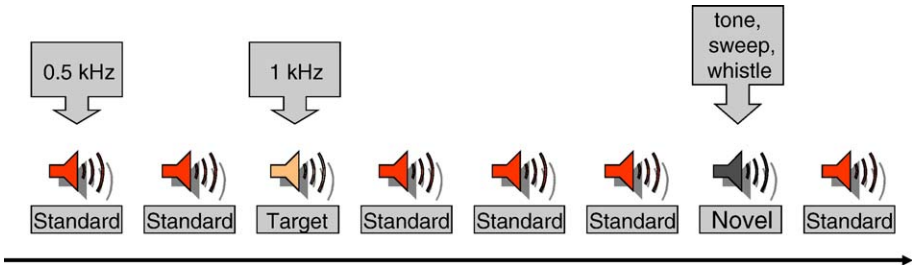

Fig. 2. Auditory oddball paradigm: auditory oddball event-related fMRI task.

stimulus duration was 200 ms with an 800, 1300, or 1800 ms interstimulus interval. All stimuli were presented at approximately 80 dB above the standard threshold of hearing. All participants reported that they could hear the stimuli and discriminate them from the background scanner noise. Prior to entry into the scanning room or ERP booth, each participant performed a practice block of 10 trials to ensure each subject understood the instructions. The participants were instructed to respond as quickly and accurately as possible with their right index finger every time they heard the target stimulus and not to respond to the nontarget stimuli or the novel stimuli. An MRI compatible fiber-optic response device (Lightwave Medical, Vancouver, B.C.) was used to acquire behavioral responses for the task in both the ERP and the fMRI experiments. The stimulus paradigm, data acquisition techniques, and previously found stimulus-related activation are described more fully elsewhere (Kiehl et al., 2005).

Data acquisition

fMRI and ERP data were acquired on the same day in two different sessions, using identical stimuli and the order of the fMRI or ERP sessions was counterbalanced between individuals, at the Olin Neuropsychiatry Research Center at the Institute of Living. The fMRI data were collected on a Siemens Allegra 3 T dedicated head scanner equipped with 40 mT/m gradients and a standard quadrature head coil. The functional scans were acquired using gradient-echo echo-planar-imaging with the following parameters (repeat time (TR) = 1.50 s, echo time (TE) = 27 ms, field of view = 24 cm, acquisition matrix = 64 × 64, flip angle = 70°, voxel size = 3.75 × 3.75 × 4 mm, gap = 1 mm, 29 slices, ascending acquisition). Six "dummy" scans were performed at the beginning to allow for longitudinal equilibrium, after which the paradigm was automatically triggered to start by the scanner. The ERP data were collected using an SA bioelectric amplifier system capable of amplifying electrical activity from 64 separate single-ended channels. Amplifiers were connected to a 16-bit A/D conversion using a custom program (Digitize) implemented on a Pentium II microcomputer running Solaris for Intel. The Digitize program recorded the EEG data and all stimulus and behavioral response codes for later analysis.

Preprocessing

fMRI data were preprocessed using the software package SPM2 (http://www.fil.ion.ucl.ac.uk/spm/). Images were realigned using INRIalign—a motion correction algorithm unbiased by local signal changes (Freire et al., 2002). Next, data were spatially normalized into standard Montreal Neurological Institute space (Friston et al., 1995), spatially smoothed with a 12 × 12 × 12 mm full width at half-maximum Gaussian kernel. The data (originally acquired at 3.75 × 3.75 × 4 mm) were slightly subsampled to 3 × 3 × 3 mm, resulting in 53 × 63 × 46 voxels.

Event-related potential recording

Scalp potentials were recorded from tin electrodes (ElectroCap International) placed over 62 electrode sites according to standard placement guidelines of the International 10–20 System and some additional sites. Vertical and horizontal electrooculograms (EOG) were monitored from electrodes located on the lateral and supra-orbital ridges of the right eye. All electrodes were referenced to the nose. Electrical impedances were maintained below 10 kΩ throughout the experiment. The EEG channels (SA instruments) were amplified (20,000 gain) with a bandpass of 0.01 to 100 Hz, digitized on-line at a rate of 500 samples per second, and recorded on computer hard disk. EEG data were preprocessed using ICA to remove ocular artifacts from the EEG data (Jung et al., 2000). Data were then digitally filtered with a 20 Hz low pass filter to reduce electromyographic activity and ERPs were constructed for trials in which participants correctly identified target stimuli. The recording epoch was 1400 ms long with a 200 ms prestimulus baseline. The infrequent stimuli have been shown to elicit a P3 response which consists of generators located anteriorly (frontal, early portion of the P3 response) as well as posteriorly (parietal, later portion of the P3 response or P3-proper). Data from a midline central site (Cz) were included in the ICA fusion analyses because it appeared to be the best single channel to detect both anterior and posterior sources (results were nearly identical when scalp site Pz was used instead of Cz).

Joint ERP/fMRI data fusion

We use an algorithm based upon the infomax principle (Bell and Sejnowski, 1995). The Infomax algorithm employs a gradient ascent algorithm to maximize the entropy of the output of a single layer neural network (Lee et al., 1999). We assume joint spatial or temporal independence of the fMRI and ERP sources, respectively, using the following generative model for the data: $\mathbf{x}^{\mathrm{F}} = \mathbf{A}\mathbf{s}^{\mathrm{F}}$ and $\mathbf{x}^{\mathrm{E}} = \mathbf{A}\mathbf{s}^{\mathrm{E}}$. For the case of two sources and two subjects, $\mathbf{x}^{\mathrm{F}} = [x_1^{\mathrm{F}}\ x_2^{\mathrm{F}}]^T$ is the mixed data for the fMRI modality for the two subjects, $\mathbf{x}^{\mathrm{E}} = [x_1^{\mathrm{E}}\ x_2^{\mathrm{E}}]^T$ is the mixed data for the ERP modality for the two subjects, $\mathbf{A} = \begin{bmatrix} a_{11} & a_{12} \\ a_{21} & a_{22} \end{bmatrix}$ is a shared linear mixing matrix, and $\mathbf{s}^{\mathrm{F}}$ and $\mathbf{s}^{\mathrm{E}}$ are the respective fMRI and ERP sources. We can write this as a single equation by forming a data vector for each subject as $\mathbf{x}_i = [x_i^{\mathrm{F}}\ x_i^{\mathrm{E}}]$, and likewise for a source vector $\mathbf{s}_i = [s_i^{\mathrm{F}}\ s_i^{\mathrm{E}}]$. The resulting update equation for the algorithm to compute the shared unmixing matrix $\mathbf{W}$ (i.e., the inverse of $\mathbf{A}$) and the fused ERP and fMRI sources, $\mathbf{u}^{\mathrm{E}}$ and $\mathbf{u}^{\mathrm{F}}$, is as follows:

$$\Delta\mathbf{W} = \eta\left\{\mathbf{I} - 2\mathbf{y}^{\mathrm{E}}\left(\mathbf{u}^{\mathrm{E}}\right)^T - 2\mathbf{I}^{\mathrm{F}}\left(\mathbf{u}^{\mathrm{F}}\right)^T\right\}\mathbf{W}, \tag{1}$$

where $\mathbf{y}^{\mathrm{E}} = g(\mathbf{u}^{\mathrm{E}})$, $\mathbf{y}^{\mathrm{F}} = g(\mathbf{u}^{\mathrm{F}})$, and $g(x) = 1 / (1 + e^{-x})$ is the nonlinearity in the neural network (Bell and Sejnowski, 1995).

Component estimation

The number of independent components in the joint data was estimated to be 12 using a method based on the minimum description length criteria (Wax and Kailath, 1985). Independent components were estimated, and ranked by their contribution to the average ERP time courses by first regressing the components onto the average ERP data, then computing the maximum absolute peak of the fitted time courses. Components which contributed greater than 1 standard deviation were interpreted (*all* components are shown in the ERP plots for Fig. 5; regions in the fMRI component were scaled to Z values and a voxel was colorized if it was greater than $Z = 3.5$). A leave one out cross-validation approach was used to assess the robustness of the results; mean results are reported.

Spatiotemporal reconstruction

The joint components (shown in Fig. 4), though a useful summary, do not show clearly how these component interact with

one another. To do this, we compute spatiotemporal "snapshots" of the significant components in two ways. First, we display all the ERP components, and compute a linear combination of the fMRI components weighted by their joint ERP time courses for a specific point in time (see Fig. 1c and Fig. 5). If the N spatial (fMRI) and temporal (ERP) components are written as $\mathbf{T} = [\mathbf{t}_1 \ldots \mathbf{t}_N]$, and $\mathbf{S} = [\mathbf{s}_1 \ldots \mathbf{s}_N]$, where $\mathbf{t}_i$ is a $T \times 1$ vector containing the ERP time points and $\mathbf{s}_i$ is a $V \times 1$ vector containing the V brain voxels, we can compute the fMRI movie as $\mathbf{M}_F = |\mathbf{T}| \times \mathbf{S}^T$—the absolute value is needed since the joint components are fused using a single weight parameter, thus a change in the amplitude of the fMRI component is directly linked to change in the ERP component by this parameter. Likewise, we compute an estimated ERP time course for a given voxel by computing $\mathbf{M}_E = \mathbf{T} \times |\mathbf{S}|^T$ (Fig. 6).

Results

Performance on the auditory oddball task for the ERP and fMRI sessions was nearly identical. Mean and standard deviations are reported for (a) reaction time (fMRI 430.7 ± 90.4 ms; ERP 431.5 ± 93.6 ms, $P > 0.9$ paired t test) and (b) accuracy for target detection (fMRI 99.5 ± 0.01%; ERP 99.5 ± 0.02%, $P > 0.99$ paired t test).

Group averaged fMRI (Fig. 3a) and ERP (Fig. 3b) results are shown for the target stimuli and are consistent with previous results (Halgren et al., 1998; Kiehl et al., 2005). The fMRI data for targets relative to standards show activity in a large amount of the brain, with local maxima in bilateral temporal lobes, inferior parietal lobe, subcortical structures such as thalamus, and motor planning and execution regions, showing similar results as our previous work (Kiehl et al., 2005). The ERP data contain the expected positive and negative peaks, N1, N2, P1, P2, P3, and slow wave (SW) (marked on the figure).

The spatial and temporal joint components for the significant components are presented in Figs. 4a–f. Significant regions of activation for the fMRI maps are shown on the left and the average ERP time course (in yellow; on all plots) is plotted along with the components (in cyan) on the right. The ERP time courses correspond remarkably well to distinct peaks present on the average time courses. Additionally, when the temporal ERP components are viewed together with the spatial fMRI maps, the spatiotemporal dynamics of the auditory oddball target response are visible. Such a view provides a useful parameterization of the oddball response. For example, the N1 peak in Fig. 4a is associated with prominent activation in thalamic and primary and secondary auditory temporal lobe regions, as well as more discrete activation in several other brain regions including the supplemental motor area. Also visible for this waveform is a late negative peak. By the N2 peak (Fig. 4b), posterior temporal lobe (heteromodal association areas), anterior cingulate, and primary motor areas are activated. Fig. 4c shows a triphasic waveform, mainly associated with bilateral temporal lobe. The early portion of the P3 component (called P3a) (Fig. 4d) is again associated with fMRI activity in thalamic regions and posterior superior parietal lobe areas. Notably, Fig. 4e, in addition to fMRI increases in temporoparietal regions, shows an fMRI signal decrease in the orbitofrontal cortex (cf. the bright blue region).

The ICA decomposition can be used to create a spatiotemporal movie to more clearly reveal the dynamic interplay between the components. Fig. 5 shows six "snapshots" for the movie created for the target stimuli (full movie available at http://www.nrc-iol.org/mialab/results.htm). On the left of each snapshot is shown a linear sum of the individual fMRI maps (Fig. 4), weighted by their respective ERP time courses at the time indicated above the figure (e.g., 84 ms). On the right of each snapshot, the average ERP waveform is again plotted as are all estimated ERP components (the six significant ones are easily visible above the flat baseline). During the peak of the first component of the ERP, the N1, the fMRI map shows hemodynamic activity in bilateral temporal lobe including superior and middle temporal gyrus (primary auditory cortex).

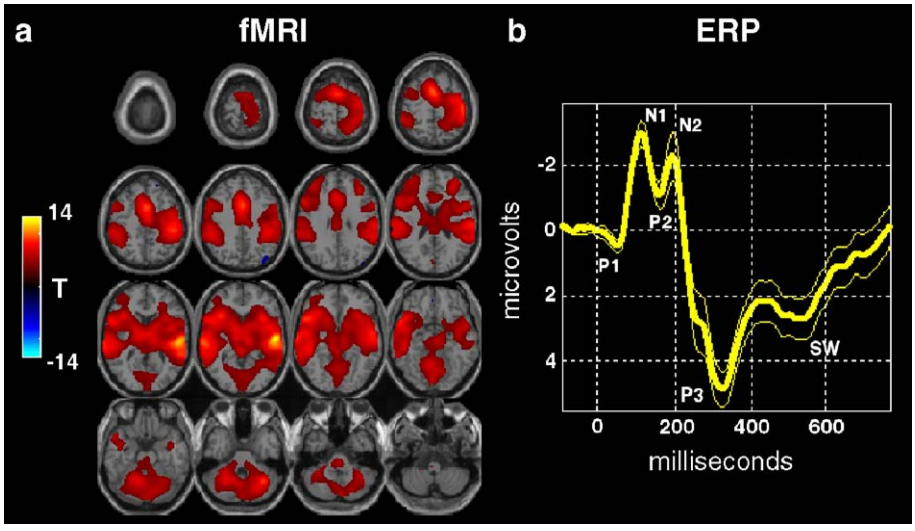

Fig. 3. Group averaged fMRI and ERP results: group fMRI (left) and ERP (right) results for the target response. The SPM2 software was used to generate a map of target-related activation for each subject. These maps are then entered into a one-sample, voxelwise t test and thresholded at $P < 0.001$ (corrected for multiple comparisons) to produce the resulting image with t values shown in color. The ERP plot was generated by averaging the data time locked to the target stimuli. Standard error is shown and peaks are labeled with the standard naming convention (e.g., P1 is the first positive peak).

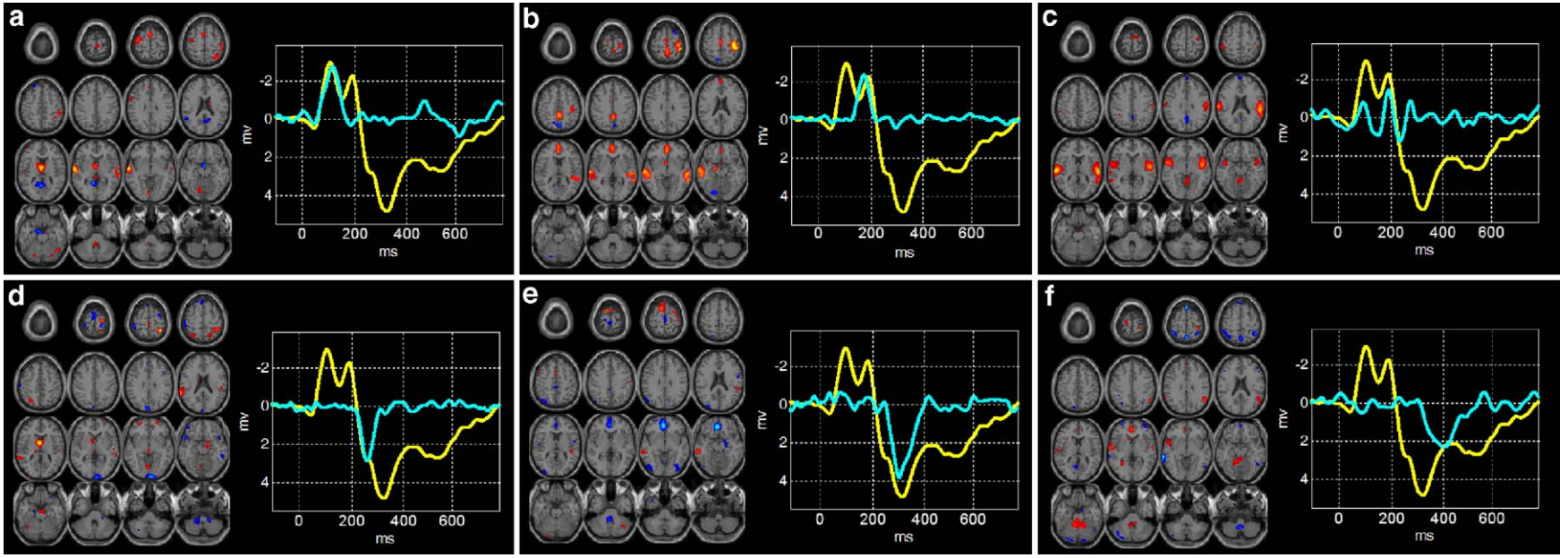

Fig. 4. ICA decomposition of ERP and fMRI joint data for target stimuli: six components were found to significantly load onto the ERP time courses. Each of these components is shown in a separate panel in the figure. The fMRI maps are thresholded at $|Z| > 3.5$ for display purposes. The average target-related ERP time course (shown also in Fig. 3b) is shown in yellow (same for all figures) and the ERP component is plotted in cyan. Positive (orange) and negative (blue) Z values are shown in the image.

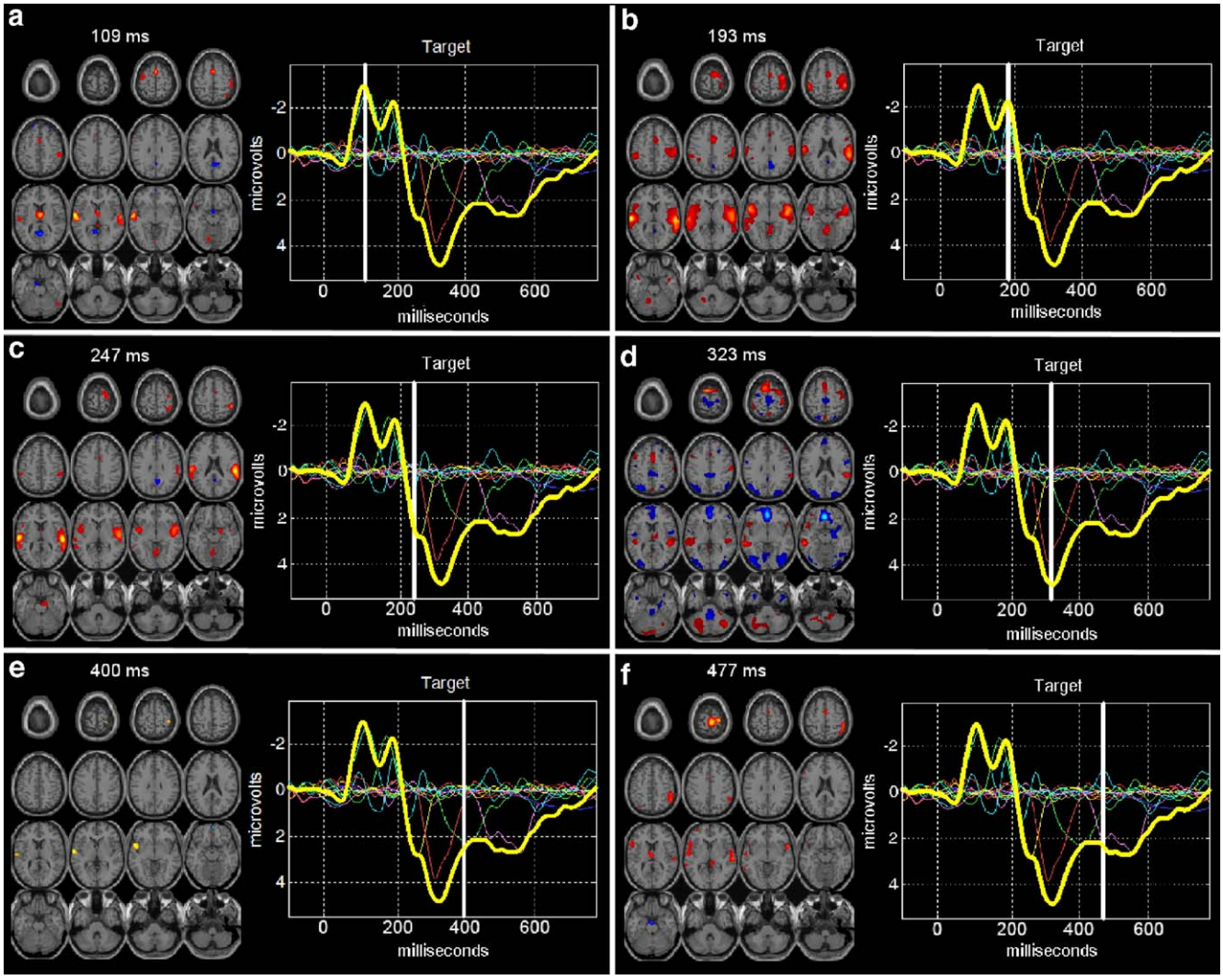

Fig. 5. ERP components and fMRI "snapshots": on the left of each window is shown a linear combination of the fMRI maps, weighted by the ERP part of the component at a specific point in time. On the right of each window is shown all of the estimated ERP components (the six shown in Fig. 4 are easily visible above the others). Such a display provides a dynamic way to visualize the results (see also movies at: http://www.nrc-iol.org/mialab/results.htm). Positive (orange) and negative (blue) Z values are shown in the image.

During the peak of the second ERP component, the N2, hemodynamic activity in both anterior superior temporal gyrus (a heteromodal sensory association region) and posterior middle/superior temporal gyrus (secondary auditory cortex) is visible. The first substantial positive component (the P3a) is fused with hemodynamic activity in multiple frontal and parietal lobe regions, in addition to bilateral temporal lobe regions.

Alternatively, we can visualize the estimated ERP time courses (i.e., linear combinations of the significant ERP components) at specific positions in the brain (Fig. 6). Notably, the regions which show the earliest maximal response (84 ms snapshot) include thalamus, primary and secondary auditory cortex, and supplemental motor area. Next, primary motor and more posterior temporal lobe regions show maximal activity during the N2 peak (211 ms snapshot). Finally, the P3 peak is associated with medial frontal lobe, brain stem, and posterior temporal lobe association regions (406 ms snapshot). Montreal Neurological Institute (MNI) coordinates (in millimeters) and anatomic labels of the plotted regions are shown in Table 1.

Discussion

We compute a spatiotemporal reconstruction of the healthy human brain's response to a well-studied auditory oddball task with high temporal and spatial resolution, using a fusion of electromagnetic and hemodynamic data. Recent work, examining correspondence between these two very different types of data has shown promising results (Logothetis et al., 2001; Vitacco et al., 2002; Horovitz et al., 2002; Mathalon et al., 2003) and suggests that methods combining the strengths of both techniques may provide new insights into human brain function. By taking advantage of interparticipant covariation between the ERP and fMRI data, a connection can be made between the two techniques by 'fusing' temporal components of the ERP time courses to spatial components of the fMRI images.

In this work, we do not attempt to explicitly utilize the temporal information in the fMRI response, nor do we use the spatial information in the ERP response. Doing so, though an attractive goal, would require making assumptions about how the spatial and/

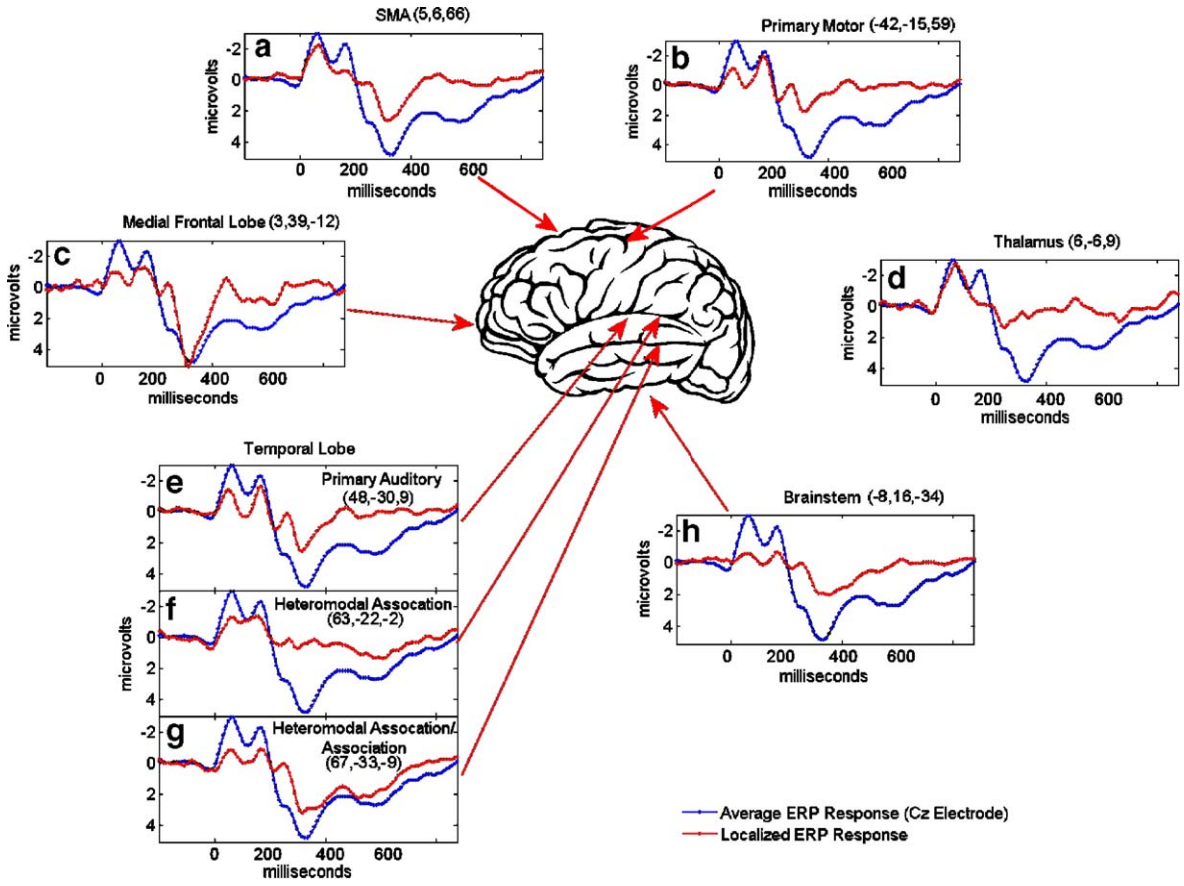

Fig. 6. Region specific ERP time courses: average (blue; same for all plots) and reconstructed (red) ERP time courses (ERP components linearly weighted by their associated fMRI components at specific voxel values) are shown for eight areas of interest (MNI coordinate are also provided for each area).

or temporal information in the two, fundamentally different, modalities is directly related (Liu et al., 1998). We instead focus upon the strengths of both techniques by fusing together the hemodynamic spatial information in the fMRI data with the electromagnetic temporal information in the ERP data by using the joint constraints of temporal (ERP) and spatial (fMRI) independence. Specifically, the independence between joint ERP and fMRI components is maximized while the intersubject covariation for the fused times (ERP) and positions (fMRI) is modeled by the linear mixing parameters.

Table 1
Coordinates for regions indicated in Fig. 6

Figure name	MNI coordinate	Anatomic label (BA[a])
Thalamus	(6, −6, 9)	Thalamus
Supplemental motor area	(5, 6, 66)	Superior frontal gyrus (BA6)
Primary auditory	(48, −30, 9)	Superior temporal gyrus (BA41)
Primary motor	(−42, −15, 59)	Precentral gyrus (BA4)
Heteromodal association 1	(63, −22, −2)	Superior temporal gyrus (BA21)
Brain stem	(−8, 16, −34)	Brain stem
Heteromodal association/association	(67, −33, −9)	Middle temporal gyrus (BA21)
Medial frontal	(3, 39, −12)	Medial frontal gyrus (BA11)

The Montreal Neurological Institute (MNI) coordinates are shown for each of the eight regions plotted in Fig. 2. The anatomic label and approximate Brodmann area (BA) is also provided.

[a] Brodmann areas (BA) are only approximate, based upon the Talairach Atlas.

For clarity, we formulate the discussion around the findings as presented in Fig. 5. The first window Fig. 5a, corresponding to the N1 peak for the ERP data, shows activity in the primary and secondary auditory regions of the temporal lobe as well as in motor planning regions. This is consistent with what we would expect following the initial auditory stimulus, and the corresponding preparatory motor activity required for the button press. The next window, corresponding to the N2 peak, shows extensive temporal lobe activation, including heteromodal association cortex. Motor planning, primary motor, and cerebellar regions are also activated in this map, consistent with regions known to be involved in the execution of the motor response. This result also corresponds with the peak of a triphasic waveform (shown in Fig. 4c), a waveform which has been shown using intracranial recording data (Halgren et al., 1995).

Fig. 5c, corresponding to the P3a peak, shows additional temporal lobe regions, somatosensory cortex, and brain stem activity, all consistent with what would be expected to be involved in the P3 signal. The brain stem activity is interesting to consider. A recent study proposed that the P3 reflects the response of the locus coeruleus norepinephrine (LC-NE) system to the outcome of internal decision making processes, and the consequent effects of noradrenergic potentiation of information processing (Nieuwenhuis et al., 2005). Such a model is not easily testable with scalp ERP

alone because of the distance from the scalp to the brainstem, the small signal produced, and inaccuracies in source localization estimates for such a small region. However, combining fMRI with ERP can reveal regions, undetected by ERPs alone, which play a participatory role. Thus, though the initial electrical activity is not visible, the association of brain stem activity with the later detected ERP P3 response is evidence supportive of a role for the LC in generating the P3. Our results are thus consistent with involvement of the LC-NE system, showing brain stem involvement during the P3 response (although our finding cannot be definitive due to the small size of the LC and the lack of definitive anatomic information).

The finding in Fig. 5d, corresponding to the later portion of the P3 response (called P3b or P3 proper), shows activity in posterior bilateral temporal and temporoparietal lobe regions in addition to lateral prefrontal areas (Soltani and Knight, 2000). Cerebellar activity is evident as well, nearly coincident with the motor response. Interesting to note are the fMRI signal decreases found in medial frontal and temporoparietal areas. This is consistent with previous studies which have shown a diminution of different portions of the P3 response following temporoparietal and frontal lesions (Yamaguchi and Knight, 1991; Spitzer et al., 1996; Rule et al., 2002). Fig. 5e shows the positive slow wave ERP activity fused with hemodynamic activity in anterior temporal lobe regions. A late waveform (shown in Fig. 5f) is consistent with a post-stimulus evaluative response (Kiehl et al., 1999). This response is contributed to by the component that was showing activity during the N1 peak (cf. Fig. 4a). This process may be related to the reorienting negativity (Schroger and Wolff, 1998) as it involved regions commonly assumed to subserve auditory attentional processes.

Our technique provides several advantages. We demonstrate an approach for combining data from fMRI and ERP modalities, each with different strengths and advantages, in a way that does not favor one modality. We perform a joint decomposition of both modalities which are linked or fused by a common mixing parameter. Our approach does not require assumptions about the number of dipoles or the solving of an inverse problem for EEG or require the use of a threshold for the fMRI data. Our approach also separates the data into joint components, each of which has an ERP and an fMRI portion. Decomposing the data into joint components may provide a useful way to examine component specific differences in, e.g., different patient groups or modified versions of the task.

The present study also has limitations. First, we are examining data from a single electrode in our analysis. In future work, we hope to extend our methods to incorporate multiple EEG electrodes as well as multiple fMRI time points. Secondly, we have used a nose reference which, although it provides some degree of control, can impact the waveform shape and the power spectra of the recorded EEG (Lehmann, 1987; Nunez, 1995). This effect may be mitigated by the use of techniques such as a surface Laplacian transformation (providing reference-free signals) (Nunez and Pilgreen, 1991). We are encouraged that the results we have found appear valid and are reliably detected in this data set; however, additional preprocessing as mentioned may improve our statistical sensitivity. Thirdly, the fMRI analysis approaches we have used, though widely used and fairly robust, may be subject to some model misfit problems. It may thus be helpful to incorporate a data-driven fMRI approach, such as ICA, to extract activation maps which can then be fused to the ERP data.

In summary, we have used a combination of electrical and hemodynamic data to visualize, in humans, the neural systems involved during different portions of the auditory "oddball" target detection response. Deep brain structures, which are likely participatory in the target response, were also implicated in our results. This work demonstrates that data fusion techniques can be successfully applied to joint ERP and fMRI data to reveal unique information by taking advantage of the primary strengths of these different modalities. We have thus been able to compute an estimate of the neuronal chronometry of target detection throughout the whole brain, using two noninvasive techniques in humans.

Acknowledgments

The authors would like to thank Jana Schaich Borg, Matthew Johnson, Laurie Skelly, Greg Book, and Alvin Chon for their help with data collection and Danny Mathalon and Wally Deckel for insightful comments. This research was supported in part by the National Institutes of Health, under grants 1 R01 EB 000840, 1 R01 EB 005846 (VDC), 1 R01 MH 0705539 (KAK), and by two Hartford Hospital Open Grant Competition Awards (VDC and KAK) and two National Alliance for Research on Schizophrenia and Depression Young Investigator Awards (VDC and KAK).

References

Arthurs, O.J., Boniface, S.J., 2003. What aspect of the FMRI BOLD signal best reflects the underlying electrophysiology in human somatosensory cortex? Clin. Neurophysiol. 114 (7), 1203–1209.

Arthurs, O.J., Williams, E.J., Carpenter, T.A., Pickard, J.D., Boniface, S.J., 2000. Linear coupling between functional magnetic resonance imaging and evoked potential amplitude in human somatosensory cortex. Neuroscience 101 (4), 803–806.

Bell, A.J., Sejnowski, T.J., 1995. An information maximisation approach to blind separation and blind deconvolution. Neural Comput. 7 (6), 1129–1159.

Brown, W.S., Marsh, J.T., Smith, J.C., 1979. Principal component analysis of ERP differences related to the meaning of an ambiguous word. Electroencephalogr. Clin. Neurophysiol. 46 (6), 709–714.

Calhoun, V.D., Kraut, M., Adali, T., Pearlson, G.D., 2000. A weighted-least squares method for latency estimation in fMRI. Proc. ISMRM Denver, CO., p. 814.

Calhoun, V.D., Adali, T., Pearlson, G.D., Pekar, J.J., 2001. Spatial and temporal independent component analysis of functional MRI data containing a pair of task-related waveforms. Hum. Brain Mapp. 13 (1), 43–53.

Clark, V.P., Fannon, S., Lai, S., Benson, R., 2001. Paradigm-dependent modulation of event-related FMRI activity evoked by the oddball task. Hum. Brain Mapp. 14 (2), 116–127.

Dale, A.M., Liu, A.K., Fischl, B.R., Buckner, R.L., Belliveau, J.W., Lewine, J.D., Halgren, E., 2000. Dynamic statistical parametric mapping: combining FMRI and MEG for high-resolution imaging of cortical activity. Neuron 26 (1), 55–67.

Debener, S., Makeig, S., Delorme, A., Engel, A.K., 2005. What is novel in the novelty oddball paradigm? Functional significance of the novelty P3 event-related potential as revealed by independent component analysis. Brain Res. Cogn. Brain Res. 22 (3), 309–321.

Dien, J., Spencer, K.M., Donchin, E., 2004. Parsing the late positive complex: mental chronometry and the ERP components that inhabit the neighborhood of the P300. Psychophysiology 41 (5), 665–678.

Donchin, E., Coles, M.G.H., 1988. Is the P300 component a manifestation of context updating? Behav. Brain Sci. 11, 357–374.

Ford, J.M., White, P., Lim, K.O., Pfefferbaum, A., 1994. Schizophrenics have fewer and smaller P300s: a single-trial analysis. Biol. Psychiatry 352, 96–103.

Freire, L., Roche, A., Mangin, J.F., 2002. What is the best similarity measure for motion correction in FMRI time series? IEEE Trans. Med. Imag. 21 (5), 470–484.

Friston, K., Ashburner, J., Frith, C.D., Poline, J.P., Heather, J.D., Frackowiak, R.S., 1995. Spatial registration and normalization of images. Hum. Brain Mapp. 2, 165–189.

Gehring, W.J., Gratton, G., Coles, M.G., Donchin, E., 1992. Probability effects on stimulus evaluation and response processes. J. Exp. Psychol. Hum. Percept. Perform. 18 (1), 198–216.

Goldman, R.I., Stern, J.M., Engel Jr., J., Cohen, M.S., 2002. Simultaneous EEG and FMRI of the alpha rhythm. NeuroReport 13 (18), 2487–2492.

Halgren, E., Baudena, P., Clarke, J.M., Heit, G., Liégeois, C., Chauvel, P., Musolino, A., 1995. Intracerebral potentials to rare target and distractor auditory and visual stimuli: I. Superior temporal plane and parietal lobe. Electroencephalogr. Clin. Neurophysiol. 94 (3), 191–220.

Halgren, E., Marinkovic, K., Chauvel, P., 1998. Generators of the late cognitive potentials in auditory and visual oddball tasks. Electroencephalogr. Clin. Neurophysiol. 106 (2), 156–164.

Horovitz, S.G., Skudlarski, P., Gore, J.C., 2002. Correlations and dissociations between BOLD signal and P300 amplitude in an auditory oddball task: a parametric approach to combining FMRI and ERP. Magn. Reson. Imaging 20 (4), 319–325.

Jung, T.P., Makeig, S., Humphries, C., Lee, T.W., McKeown, M.J., Iragui, V., Sejnowski, T.J., 2000. Removing electroencephalographic artifacts by blind source separation. Psychophysiology 37 (2), 163–178.

Kayser, J., Tenke, C.E., 2003. Optimizing PCA methodology for ERP component identification and measurement: theoretical rationale and empirical evaluation. Clin. Neurophysiol. 114 (12), 2307–2325.

Kayser, J., Tenke, C.E., Bruder, G.E., 1998. Dissociation of brain ERP topographies for tonal and phonetic oddball tasks. Psychophysiology 35 (5), 576–590.

Kiehl, K.A., Liddle, P.F., 2001. An event-related functional magnetic resonance imaging study of an auditory oddball task in schizophrenia. Schizophr. Res. 48 (2–3), 159–171.

Kiehl, K.A., Hare, R.D., Liddle, P.F., McDonald, J.J., 1999. Reduced P300 responses in criminal psychopaths during a visual oddball task. Biol. Psychiatry 45 (11), 1498–1507.

Kiehl, K.A., Laurens, K.R., Duty, T.L., Forster, B.B., Liddle, P.F., 2001. Neural sources involved in auditory target detection and novelty processing: an event-related FMRI study. Psychophysiology 38 (1), 133–142.

Kiehl, K.A., Stevens, M., Laurens, K.R., Pearlson, G.D., Calhoun, V.D., Liddle, P.F., 2005. An adaptive reflexive processing model of neurocognitive function: supporting evidence from a large scale (n = 100) FMRI study of an auditory oddball task. NeuroImage 25, 899–915.

Knight, R.T., Nakada, T., 1998. Cortico-limbic circuits and novelty: a review of EEG and blood flow data. Rev. Neurosci. 9 (1), 57–70.

Lee, T.W., Girolami, M., Sejnowski, T.J., 1999. Independent component analysis using an extended infomax algorithm for mixed subgaussian and supergaussian sources. Neural Comput. 11, 417–441.

Lehmann, D., 1987. Principles of Spatial Analysis. Handbook of Electroencephalography and Clinical Neurophysiology. Elsevier, Amsterdam, pp. 309–354.

Liu, A.K., Belliveau, J.W., Dale, A.M., 1998. Spatiotemporal imaging of human brain activity using functional MRI constrained magnetoencephalography data: Monte Carlo simulations. Proc. Natl. Acad. Sci. U. S. A. 95 (15), 8945–8950.

Logothetis, N.K., Pauls, J., Augath, M., Trinath, T., Oeltermann, A., 2001. Neurophysiological investigation of the basis of the FMRI signal. Nature 412 (6843), 150–157.

Makeig, S., Jung, T.P., Bell, A.J., Ghahremani, D., Sejnowski, T.J., 1997. Blind separation of auditory event-related brain responses into independent components. Proc. Natl. Acad. Sci. 94 (20), 10979–10984.

Martinez-Montes, E., Valdes-Sosa, P.A., Miwakeichi, F., Goldman, R.I., Cohen, M.S., 2004. Concurrent EEG/FMRI analysis by multiway partial least squares. NeuroImage 22 (3), 1023–1034.

Mathalon, D.H., Whitfield, S.L., Ford, J.M., 2003. Anatomy of an error: ERP and FMRI. Biol. Psychol. 64 (1–2), 119–141.

McCarley, R.W., Faux, S.F., Shenton, M.E., Nestor, P.G., Adams, J., 1991. Event-related potentials in schizophrenia: their biological and clinical correlates and a new model of schizophrenic pathophysiology. Schizophr. Res. 4 (2), 209–231.

McCarthy, G., Luby, M., Gore, J., Goldman-Rakic, P., 1997. Infrequent events transiently activate human prefrontal and parietal cortex as measured by functional MRI. J. Neurophysiol. 77 (3), 1630–1634.

McKeown, M.J., Makeig, S., Brown, G.G., Jung, T.P., Kindermann, S.S., Bell, A.J., Sejnowski, T.J., 1998. Analysis of FMRI data by blind separation into independent spatial components. Hum. Brain Mapp. 6, 160–188.

Menon, V., Ford, J.M., Lim, K.O., Glover, G.H., Pfefferbaum, A., 1997. Combined event-related FMRI and EEG evidence for temporal–parietal cortex activation during target detection. NeuroReport 8 (14), 3029–3037.

Naatanen, R., Alho, K., 1995. Mismatch negativity—A unique measure of sensory processing in audition. Int. J. Neurosci. 80 (1–4), 317–337.

Nieuwenhuis, S., Aston-Jones, G., Cohen, J.D., 2005. Decision making, the P3, and the locus coeruleus-norepinephrine system. Psychol Bull. 131, 510–532.

Nunez, P.L., 1995. Neocortical Dynamics and Human EEG Rhythms. Oxford Univ. Press, New York.

Nunez, P.L., Pilgreen, K.L., 1991. The spline-laplacian in clinical neurophysiology: a method to improve EEG spatial resolution. J. Clin. Neurophysiol. 8 (4), 397–413.

Opitz, B., Mecklinger, A., von Cramon, D.Y., Kruggel, F., 1999. Combining electrophysiological and hemodynamic measures of the auditory oddball. Psychophysiology 36 (1), 142–147.

Polich, J., Kok, A., 1995. Cognitive and biological determinants of P300: an integrative review. Biol. Psychol. 41 (2), 103–146.

Rule, R.R., Shimamura, A.P., Knight, R.T., 2002. Orbitofrontal cortex and dynamic filtering of emotional stimuli. Cogn. Affect Behav. Neurosci. 2 (3), 264–270.

Saad, Z.S., Ropella, K.M., Cox, R.W., DeYoe, E.A., 2001. Analysis and use of FMRI response delays. Hum. Brain Mapp. 13 (2), 74–93.

Schroger, E., Wolff, C., 1998. Attentional orienting and reorienting is indicated by human event-related brain potentials. NeuroReport 9 (15), 3355–3358.

Soltani, M., Knight, R.T., 2000. Neural origins of the P300. Crit. Rev. Neurobiol. 14 (3–4), 199–224.

Spitzer, R.L., Williams, J.B., Gibbon, M., 1996. Structured Clinical Interview for DSM-IV: Non-patient Edition (SCID-NP). Biometrics Research Department, New York State Psychiatric Institute, New York.

Sutton, S., Tueting, P., Zubin, J., John, E.R., 1967. Information delivery and the sensory evoked potential. Science 155 (768), 1436–1439.

Vitacco, D., Brandeis, D., Pascual-Marqui, R., Martin, E., 2002. Correspondence of event-related potential tomography and functional magnetic resonance imaging during language processing. Hum. Brain Mapp. 17 (1), 4–12.

Wax, M., Kailath, T., 1985. Detection of signals by information theoretic criteria. IEEE Trans. Acoust. Speech Signal Process. 33, 387–392.

Yamaguchi, S., Knight, R.T., 1991. Anterior and posterior association cortex contributions to the somatosensory P300. J. Neurosci. 11 (7), 2039–2054.